Coupled Cation and Charge Ordering in the $CaMn_3O_6$ Tunnel Structure

Joke Hadermann,*[,†,‡] Artem M. Abakumov,[†,§] Lisa J. Gillie,[‡,||] Christine Martin,[‡,⊥] and Maryvonne Hervieu[‡]

EMAT, University of Antwerp, Groenenborgerlaan 171, 2020 Antwerp, Belgium, Laboratoire de cristallographie et sciences des matériaux, Ecole Nationale Supérieure d'Ingenieurs de Caen, UMR CNRS 6508, ISMRA-ENSICAEN, France, Department of Chemistry, Moscow State University, Moscow 119992, Russia, Department of Chemical and Biological Sciences, School of Applied Sciences, University of Huddersfield, Queensgate, Huddersfield H1 3DH, United Kingdom, and ISIS, CCLRC Rutherford Appleton Laboratory, Chilton-Didcot OX11 0QX, United Kingdom

Received August 11, 2006. Revised Manuscript Received September 7, 2006

The synthesis and crystal structure of a mixed valent manganite $CaMn_3O_6$, equivalent to $Ca_{2/3}Mn_2O_4$, are reported, along with the magnetic properties. The structure was determined using electron diffraction and high-resolution transmission electron microscopy and refined from X-ray and neutron powder diffraction data ($a = 10.6940(3)$ Å, $b = 11.3258(3)$ Å, $c = 8.4881(2)$ Å, $\beta = 122.358(2)°$, space group $P2_1/a$, $R_I = 0.037$, $R_P = 0.118$). The structure is based on a framework of double chains of edge-sharing MnO_6 octahedra. The corner-sharing chains form a framework with six-sided tunnels, identical to that of the $CaFe_2O_4$ structure. The Ca^{2+} cations are located in the tunnels. Compared to $CaFe_2O_4$, one-third of the Ca positions in the tunnels remain vacant, with an ordered distribution of vacant and occupied sites. The empty sites in neighboring Ca chains are shifted relative to each other along the *c*-axis by one period of the $CaFe_2O_4$ subcell, which results in a symmetry decrease from orthorhombic to monoclinic. Based on the interatomic Mn−O distances, the charge ordering in $CaMn_3O_6$ is discussed. The compound exhibits a strong anti-ferromagnetic character, and differences between the zfc and fc magnetization curves at low temperature suggest ferro- or ferrimagnetic interactions.

1. Introduction

The crystal chemistry of the A_xMnO_2 (A = alkali and/or alkaline-earth element) phases appears to be extremely rich and complex if we consider the large number of papers that have been devoted to these phases. Some aspects of the crystal chemistry of the AM_2O_4 oxides with tunnel structures have been reviewed by Müller-Buschbaum.[1] The major structural unit for these compounds is the rutile-type chain of edge-sharing MnO_6 octahedra. A large variety of structural types arise due to the ability of these chains to form double and triple chains by the sharing of common edges of the MnO_6 octahedra. The chains are then combined into three-dimensional frameworks by sharing common corners and/or edges. As a result, tunnels of various configurations appear in such frameworks. The smallest rutile-type tunnels are too small to accommodate the A-cations. The square hollandite-type tunnels and the six-sided tunnels of the AM_2O_4 structures incorporate one column of A-cations. For the AM_2O_4 composition, three structure models are commonly considered, namely, $CaTi_2O_4$,[2] $CaMn_2O_4$,[3] and $CaFe_2O_4$[4] (Figure 1). However, note that $CaTi_2O_4$ crystallizes in a *Bbmm* space group and $CaMn_2O_4$ in a *Pmab* space group (which is a subgroup of the first one) and that both exhibit a similar herringbone-like orientation of the double chains of edge-sharing MnO_6 octahedra, whereas the connectivity of the double chain is different in $CaFe_2O_4$. The larger "figure-of-eight" and S-shaped tunnels of the $SrMn_3O_6$,[5] $Ba_6Mn_{24}O_{48}$,[6] $CaMn_4O_8$,[7] and $Na_4Mn_9O_{18}$[8,9] structures can accommodate two to four A-cationic columns.

Tunnels of different types are often present in the same structure in an ordered way, giving rise to complicated superstructures. The situation is additionally complex due to the formation of cationic vacancies at the A-sites, which tend to be ordered, often resulting in compositionally driven incommensurately modulated structures.[5] Large infinite tunnels, which are able to host different A-cations, make these materials potential ionic conductors and matrixes for the storage of radioactive waste. In fact, the existence and

* To whom correspondence should be addressed. Joke Hadermann, University of Antwerp, Groenenborgerlaan 171, 2020 Antwerp, Belgium. Tel.:+32 32653245. Fax: +32 32653257. E-mail: joke.hadermann@ua.ac.be.
† University of Antwerp.
‡ UMR CNRS 6508, ISMRA-ENSICAEN.
§ Moscow State University.
|| University of Huddersfield.
⊥ CCLRC Rutherford Appleton Laboratory.

(1) Müller-Buschbaum, Hk. *J. Alloys Compd.* **2003**, *349*, 49.
(2) Bertaut, F.; Blum, P. *J. Phys.* **1956**, *17*, 517.
(3) Giesber, H. G.; Pennington, W. T.; Kolis, J. W. *Acta Crystallogr.* **2001**, *C57*, 329.
(4) Becker, D. F.; Casper, J. S. *Acta Crystallogr.* **1957**, *10*, 332.
(5) Gillie, L. J.; Hadermann, J.; Perez, O.; Martin, C.; Hervieu, M.; Suard, E. *J. Solid State Chem.* **2004**, *177*, 3383.
(6) Boullay, Ph.; Hervieu, M.; Raveau, B. *J. Solid State Chem.* **1997**, *132*, 239.
(7) Barrier, N.; Michel, C.; Maignan, A.; Hervieu, M.; Raveau, B. *J. Mater. Chem.* **2005**, *15*, 386.
(8) Parant, J.-P.; Olazcuaga, R.; Devalette, M.; Fouassier, C.; Hagenmuller, P. *J. Solid State Chem.* **1971**, *3*, 1.
(9) Floros, N.; Michel, C.; Hervieu, M.; Raveau, B. *J. Solid State Chem.* **2001**, *162*, 34.

10.1021/cm0618998 CCC: $33.50
Published on Web 10/14/2006

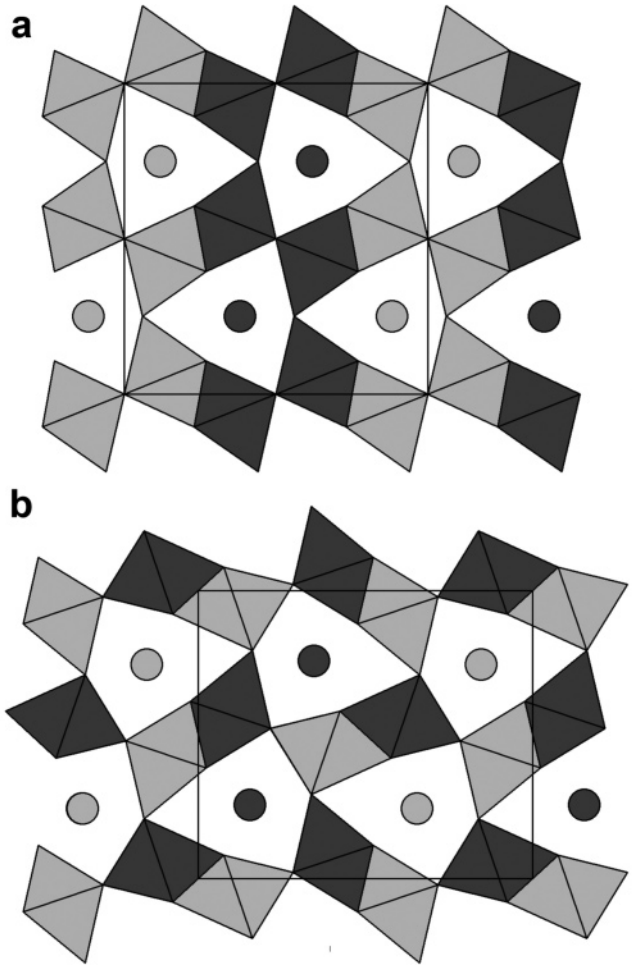

Figure 1. Projections of the two AM_2O_4-type structures: (a) $CaTi_2O_4$ and the distorted $CaMn_2O_4$ form; (b) $CaFe_2O_4$. M cations are located at the shaded octahedra, and A-cations are shown as circles. Differently shaded octahedra and cationic columns are shifted with respect to each other by one-half of the repeat period along the tunnels.

stability of tunnel and layer structures lead to well-known problems that were discussed 30 years ago in the alkaline-earth manganites, as well as their relationships with electrical and magnetic properties.[2,10]

In the manganese-rich part of the Ca−Mn−O system, three Ca_xMnO_2 compounds were reported: $CaMn_2O_4$, $CaMn_3O_6$, and $CaMn_4O_8$. The structure of $CaMn_2O_4$ has been carefully studied by different authors, who have determined the crystallographic and magnetic structure.[11−13] $CaMn_4O_8$ [7] also has a tunnel structure, but it consists of single and triple chains of edge-sharing MnO_6 octahedra, interconnected through the corners. The $[Mn_4O_8]_\infty$ framework gives rise to three types of tunnels: empty rutile-like tunnels and six-sided and eight-sided ("figure-of-eight") tunnels where the Ca^{2+} cations are situated. No crystal structure has been determined until now for the $CaMn_3O_6$ compound; only the powder X-ray diffraction (XRD) pattern and magnetic properties were reported.[14,15]

In this paper we report on the synthesis and the structural characterization of the mixed valent manganite $CaMn_3O_6$, using transmission electron microscopy and X-ray and neutron diffraction techniques. It is shown that it exhibits a $CaFe_2O_4$-like arrangement of the double rutile ribbons and an ordered distribution of Ca and cationic vacancies along the tunnels. The geometry of the MnO_6 octahedra also clearly indicate differences in the Mn−O distances, which are related to the ordering of the Ca and cationic vacancies at the A-type sublattice. The role of the manganese valence, and the size and nature of the cations inserted in the tunnels, is discussed.

2. Experimental Section

Stoichiometric proportions of high-purity CaO, MnO_2, and Mn (1:2.5:0.5) were intimately ground in an agate mortar until a homogeneous powder was achieved. This mixture was compacted into bars and placed into a re-crystallized alumina finger, which was sealed into an evacuated silica tube. The tube was then heated to 1200 °C for 12 h and then slowly cooled to ambient temperature.

Sample quality was checked using X-ray powder diffraction (XRD) (Philips vertical diffractometer with Cu Kα radiation). A longer data set, suitable for Rietveld refinement, was collected over 12 h with a step size of 0.02° over the 2θ range of 5−110°. The crystal structure determination and Rietveld refinement were performed with the JANA2000 program.[16]

Time-of-flight neutron powder diffraction (NPD) data were collected at room temperature on the General Materials Diffractometer (GEM) at the ISIS pulsed neutron source. Measurements were performed on the sample with an overall mass of ∼0.4 g, placed in a vanadium container (note that the amount of powder is small but sufficient for recording an exploitable neutron diffraction pattern). Four data banks (at 44.7°, $\Delta Q/Q \approx 0.017$; at 74.4°, $\Delta Q/Q \approx 0.008$; at 103.9°, $\Delta Q/Q \approx 0.005$; at 149.5°, $\Delta Q/Q \approx 0.003$) covering *d*-spacing ranging from 0.44 to 5.1 Å were used for the structure refinement. Rietveld refinement was performed with the GSAS/EXPGUI suite.[17,18]

The sample purity check by transmission electron microscopy (TEM) and the reconstruction of reciprocal space were carried out on a JEOL 2010 microscope. High-resolution electron microscopy (HREM) was performed with a JEOL4000EX microscope. The untwinned [010] electron diffraction (ED) pattern was recorded on a JEOL 3000FX with CCD camera. Calculated HREM images were obtained using the MacTempas software. Energy dispersive spectroscopy (EDS) analysis was done on the JEOL 2010 equipped with the Oxford Inca system.

The magnetization was measured by using a Quantum Design PPMS-VSM. Both zero field cooled (zfc) and field cooled (fc) data were collected in an applied field of 0.1 T and with increasing temperature.

3. Results

The sample was studied by electron diffraction to determine the approximate cell parameters and the possible space

(10) Fouassier, C.; Delmas, C.; Hagenmuller, P. *Mater. Res. Bull.* **1975**, *10*, 443.
(11) Giesber, H. G.; Pennington, W. T.; Kolis, J. W. *Acta Crystallogr.* **2001**, *C57*, 329.
(12) Ling, C.; Neumeir, J. J.; Argyriou, D. N. *J. Solid State Chem.* **2001**, *160*, 167.
(13) Zouari, S.; Ranno, L.; Cheikh-Rouhou, A.; Isnard, O.; Pernet, M.; Wolfers, P.; Strobel, P. *J. Alloys Compd.* **2003**, *353*, 5.
(14) Horowitz, H. S.; Longo, J. M. *Mater. Res. Bull.* **1978**, *13*, 1359.
(15) Glaunsinger, W. S.; Horowitz, H. S.; Longo, J. M.; Chang, A. *J. Solid State Chem.* **1980**, *35*, 187.
(16) Petricek, V.; Dusek, M. *JANA2000: Programs for Modulated and Composite Crystals*; Institute of Physics: Praha, Czech Republic, 2000.
(17) Larson, A. C.; Von Dreele, R. B. *LAUR 86-748*; Los Alamos National Laboratory: Los Alamos, NM, 1994.
(18) Toby, B. H. *J. Appl. Crystallogr.* **2001**, *34*, 210.

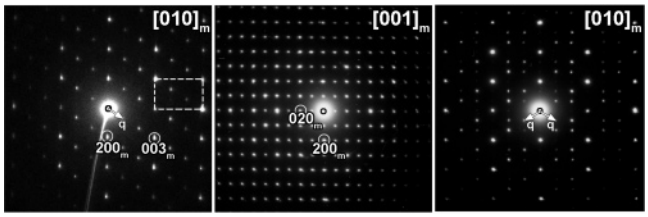

Figure 2. Electron diffraction patterns of the [010]* and [001]* zones for the $CaMn_3O_6$ material (a, b). The [010]* pattern observed in twinned crystals (c). The modulation vector **q** is indicated by a white arrow. The reflections of the orthorhombic subcell are clarified by a white rectangle.

groups. The reciprocal space was reconstructed by tilting the crystal around the crystallographic axes. The ED patterns of the [010]* and [001]* zones of $CaMn_3O_6$ are shown in Figure 2a,b. The reflections on these patterns can be divided into two groups with a clear difference in brightness: the brighter reflections belong to a subcell (outlined in white in the [010]* ED pattern) and the weaker spots are considered as superlattice reflections. The pattern of basic cell reflections is clarified by the white rectangle on the left ED pattern. The subcell reflections can be indexed using the cell parameters $a_o \approx 9.07$ Å, $b_o \approx 11.3$ Å, $c_o \approx 2.83$ Å (the subscript "o" denotes the orthorhombic subcell). This subcell is very similar to the unit cells of $CaMn_2O_4$[3] (space group *Pmab*, $a = 9.677$ Å, $b = 9.988$ Å, $c = 3.155$ Å) and $CaFe_2O_4$ [4] (space group *Pnam*, $a = 9.230$ Å, $b = 10.705$ Å, $c = 3.024$ Å). The superstructure can be described as a modulated one with a_o, b_o, and c_o as the lattice vectors for the basic structure with a modulation vector $q = {}^2/_3 a_o^* + {}^1/_3 c_o^*$ (q vector is indicated on the ED pattern). Since the modulation is commensurate, a decrease in symmetry down to a monoclinic cell can be considered for a supercell. The basic vectors of the monoclinic reciprocal supercell were chosen considering the following nodes $100_m = 100_o$, $010_m = 010_o$, and $001_m = {}^2/_3\ 0\ {}^{-1}/_{3o}$. The relationships of the lattice vectors of the orthorhombic subcell and the monoclinic supercell is given by the matrix relation

$$(a_m, b_m, c_m) = (a_o, b_o, c_o)\begin{bmatrix} 1 & 0 & 0 \\ 0 & 1 & 0 \\ 2 & 0 & -3 \end{bmatrix}$$

that results in the cell parameters $a_m \approx 10.7$ Å, $b_m \approx 11.3$ Å, $c_m \approx 8.5$ Å, and $\beta \approx 122°$ (subscript "m" represents the monoclinic supercell). This supercell is in agreement with that determined earlier by Glaunsinger et al.[15] also using electron diffraction ($a_m \approx 10$ Å, $b_m \approx 12$ Å, $c_m \approx 8$ Å, and $\beta \approx 120°$).

The reflection conditions were determined by making a tilt series and are *hkl*: no conditions, *h*0*l*: $h = 2n$, and 0*k*0: $k = 2n$. The presence of the 0*k*0: $k \neq 2n$ on the [001]* ED pattern is due to double diffraction, as these spots were seen to vanish when tilting the crystal around the *b*-axis. These reflection conditions leave $P2_1/a$ as the only possible space group. The third pattern (Figure 2c) shows a twinned [010]* pattern of the monoclinic superstructure, as evidenced by the two mirror-related directions of the modulation vectors. All crystals viewed along this direction showed this type of twinning, suggesting that the size of the twinned domains is in the nanometer range.

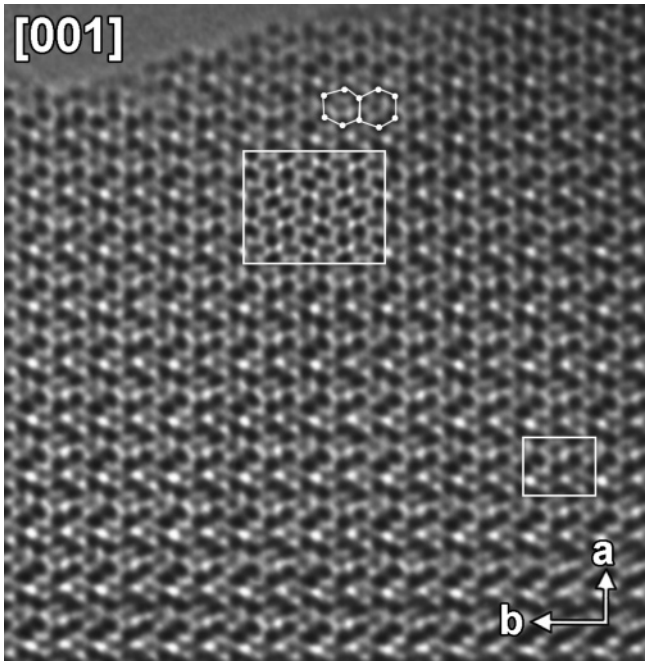

Figure 3. HREM image of $CaMn_3O_6$, taken along the [001] direction. The calculated image ($\Delta f = -330$ Å, $t = 54$ Å) is shown as an inset with a white border. The smaller white rectangle outlines one projected unit cell. Two six-sided channels are indicated on the image.

The close resemblance between the subcell of $CaMn_3O_6$ and those of $CaMn_2O_4$ and $CaFe_2O_4$ allows us to assume that the compound exhibits a tunnel structure. A HREM image of $CaMn_3O_6$ along the [001] direction is shown in Figure 3. This direction allows us to observe the projection of the tunnels and determine the arrangement of the cation columns surrounding the tunnels. High scattering density areas in the structure are depicted as dark areas on the HREM image. It can be seen that the $CaMn_3O_6$ structure shows an arrangement of six-sided tunnels; the Mn columns are indicated on the image by white dots connected with a line around the tunnel. Comparison with the tunnel structure HREM images of, for example, $CaMn_4O_8$ [7] allows us to correlate the grey areas at the centers of the hexagons with Ca^{2+} cations that occupy the tunnels. The image will be discussed further after the refinement of the structural model.

The cation composition of the sample was measured using EDS analysis and gave a Mn/Ca ratio of 3.0 (±0.1), corresponding exactly to the nominal cation composition and in agreement with the previous papers.[14,15]

The X-ray powder diffraction pattern of $CaMn_3O_6$ was indexed in a monoclinic lattice, with the cell parameters $a = 10.6940(3)$ Å, $b = 11.3258(3)$ Å, $c = 8.4881(2)$ Å, and $\beta = 122.358(2)°$, as was determined using electron diffraction. The extinction conditions observed from the X-ray powder diffraction pattern are also in agreement with the space group $P2_1/a$. Two structural models appeared to be suitable for the Rietveld refinement, based on either the $CaMn_2O_4$ or $CaFe_2O_4$ crystal structure. Both compounds show a subcell close to that of $CaMn_3O_6$, and the $P2_1/a$ space group is a subgroup of both space groups *Pmab* (space symmetry of $CaMn_2O_4$) and *Pnam* (space symmetry of $CaFe_2O_4$). In both structures, the six-sided tunnels are present (see Figure 1), with the manganese cations having the

arrangement as proposed from the HREM observations for $CaMn_3O_6$. The models differ by the scheme of connection of the double octahedral chains, i.e., mainly by the positions of the oxygen atoms.

The atomic positions of the $CaMn_2O_4$ and $CaFe_2O_4$ structures were transformed to the monoclinic $P2_1/a$ unit cell of $CaMn_3O_6$. All atoms obtained after the transformation were situated at common 4e positions of the $P2_1/a$ space group. In the transformed structures there are three positions available for Ca at (0.25, 0.33, *z*): Ca1 at $z \approx 0.55$, Ca2 at $z \approx 0.92$, and Ca3 at $z \approx 0.25$. If the occupancy factors for these positions at fixed $U_{iso} = 0.015$ Å^2 are allowed to be refined subsequently, it produced the occupancy factors g(Ca1) = 0.96(2), g(Ca2) = 0.99(2), and g(Ca3) = 0.026(8). Subsequent refinement of the atomic displacement parameters (ADPs) resulted in $U_{iso} = 0.01-0.006$ Å^2 for the Ca1 and Ca2 positions and a physically unrealistic $U_{iso} = 0.21$ Å^2 for the Ca3 position. This clearly shows that the Ca3 position is vacant; the occupancies of the Ca1 and Ca2 positions are then fixed to 1 to satisfy the cation composition $CaMn_3O_6$. Further refinement of the $CaMn_2O_4$ model resulted in a high value of the reliability factor $R_I = 0.109$ and unrealistic interatomic Mn−O distances. A much lower reliability factor $R_I = 0.037$ and reasonable structural data were obtained for the $CaFe_2O_4$ model. It should be noted that the refinement was performed without any constraints imposed on the atomic coordinates (only the ADPs were constrained to be equal for all Ca positions and all Mn positions, respectively, the ADPs for the oxygens were fixed to $U_{iso} = 0.015$ Å^2). In this particular case, the large amount of atomic positions which are independent in the monoclinic supercell but are symmetrically related in the orthorhombic subcell, together with the extensive overlap of the reflections, produce significant correlations between the refineable parameters. Taking into account the low sensitivity to the positions of oxygen atoms of conventional powder XRD, large uncertainties in the atomic coordinates for the oxygens resulted. To improve the precision of the determination of the oxygen positions, further refinement of this model was performed from NPD data. A narrow region at $d = 2.14$ Å was excluded from the refinement since it contained a small peak originating from the vanadium container. To reduce the correlations arising due to a large number of independent atomic positions, the ADPs were constrained to be equal for all atoms. The refined value of the overall ADP was equal to $U_{iso} = 0.0022(2)$ Å^2. The resulting atomic coordinates are in agreement with those refined from powder XRD data. The crystallographic parameters for $CaMn_3O_6$ are listed in Table 1, the atomic coordinates are listed in Table 2, and selected interatomic distances are shown in Table 3. The experimental, calculated, and difference NPD profiles are shown in Figure 4.

The atomic coordinates refined from the NPD data were used as input for the calculation of theoretical high-resolution electron microscopy images. The result is shown on the image of the [001] zone in Figure 3 and of the [010] zone in Figure 5. The simulations are outlined by a white border. For Figure 3, the best agreement was found at values of focus $\Delta f = -330$ Å and thickness $t = 54$ Å. At these values the cation columns are depicted as dark areas. The six-sided tunnels indicated on the image correspond to the positions of the manganese ions; Ca columns are found at the centers of these hexagons, as was already assumed by comparison of the HREM image of $CaMn_3O_6$ with other HREM images of typical tunnel structures. For Figure 5, the best agreement was found at values of focus $\Delta f = +300$ Å and thickness $t = 40$ Å. A Fourier transform of this area is given as an inset to show that this area is really untwinned. A good agreement

Table 1. Crystallographic Information for $CaMn_3O_6$ after Refinement from Powder NPD Data

composition	$CaMn_3O_6$
space group	$P2_1/a$
a (Å)	10.6956(2)
b (Å)	11.3242(2)
c (Å)	8.4901(1)
b (deg)	122.384(1)
V (Å^3)	868.38(2)
Z	8
calc. density (g cm^{-3})	4.601
no. of reflns	10670
total no. of refined params	104
no. of refined crystallographic params	65
χ^2, R_P, R_{wP}	6.69, 0.024, 0.026

Table 2. Atomic Coordinates for $CaMn_3O_6$ as Refined from Powder NPD Data

atom	*x*/*a*	*y*/*b*	*z*/*c*
Ca1	0.2381(6)	0.3325(7)	0.5459(8)
Ca2	0.2482(6)	0.3340(6)	0.9415(8)
Mn1	0.0590(10)	0.1103(8)	0.4599(14)
Mn2	0.4311(10)	0.6228(6)	0.8548(11)
Mn3	0.0789(11)	0.5922(8)	0.4668(15)
Mn4	0.4082(11)	0.0904(9)	0.8654(12)
Mn5	0.0733(9)	0.1036(7)	0.7919(12)
Mn6	0.0860(13)	0.5943(9)	0.8052(14)
O1	0.2932(7)	0.6433(5)	0.6027(8)
O2	0.1971(6)	0.1655(4)	0.7075(7)
O3	0.3875(7)	0.9806(5)	0.6819(8)
O4	0.1166(8)	0.4762(5)	0.6667(9)
O5	0.4593(7)	0.1996(2)	0.7278(8)
O6	0.0222(6)	0.6888(5)	0.6029(8)
O7	0.0681(8)	0.9136(6)	0.4556(10)
O8	0.4268(7)	0.4121(6)	0.8713(10)
O9	0.2865(7)	0.6481(5)	0.9441(8)
O10	0.3660(6)	0.9855(5)	0.9960(8)
O11	0.4642(7)	0.2016(5)	0.0618(9)
O12	0.0719(7)	0.9193(5)	0.7984(9)

Table 3. Most Relevant Interatomic Distances (Å) and Octahedral Distortion Parameters Δd for $CaMn_3O_6$

Ca1−O1	2.417(9)	Mn1−O1	1.96(1) ×1	Mn4−O2	2.09(1) ×1
Ca1−O2	2.509(9) ×1	Mn1−O2	1.92(1) ×1	Mn4−O3	1.91(1) ×1
Ca1−O3	2.362(9) ×1	Mn1−O6	2.39(1) ×1	Mn4−O5	1.97(1) ×1
Ca1−O4	2.611(10) ×1	Mn1−O7	2.23(1) ×1	Mn4−O10	1.84(1) ×1
Ca1−O5	2.516(9) ×1	Mn1−O7	1.87(1) ×1	Mn4−O10	2.22(1) ×1
Ca1−O6	2.374(7) ×1	Mn1−O12	1.90(1) ×1	Mn4−O11	1.91(1) ×1
Ca1−O7	2.274(10) ×1	⟨Mn1−O⟩	2.05	⟨Mn4−O⟩	1.99
Ca1−O8	2.558(9) ×1	Δd	0.9×10^{-2}	Δd	0.4×10^{-2}
		Mn2−O1	1.85(1) ×1	Mn5−O2	1.94(1) ×1
Ca2−O2	2.593(9) ×1	Mn2−O8	2.392(8) ×1	Mn5−O5	2.458(9) ×1
Ca2−O4	2.549(9) ×1	Mn2−O8	2.02(1) ×1	Mn5−O7	1.83(1) ×1
Ca2−O5	2.642(7) ×1	Mn2−O9	2.08(1) ×1	Mn5−O8	2.02(1) ×1
Ca2−O8	2.451(9) ×1	Mn2−O11	2.21(1) ×1	Mn5−O9	1.98(1) ×1
Ca2−O9	2.429(9) ×1	Mn2−O12	1.87(1) ×1	Mn5−O12	2.09(1) ×1
Ca2−O10	2.326(9) ×1	⟨Mn2−O⟩	2.07	⟨Mn5−O⟩	2.05
Ca2−O11	2.471(9) ×1	Δd	1.3×10^{-2}	Δd	0.9×10^{-2}
Ca2−O12	2.227(9) ×1	Mn3−O1	2.02(1) ×1	Mn6−O3	1.99(1) ×1
		Mn3−O3	1.95(1) ×1	Mn6−O4	1.92(1) ×1
		Mn3−O4	2.01(1) ×1	Mn6−O6	1.82(1) ×1
		Mn3−O4	1.93(1) ×1	Mn6−O9	1.91(1) ×1
		Mn3−O5	1.91(1) ×1	Mn6−O10	1.92(1) ×1
		Mn3−O6	1.91(1) ×1	Mn6−O11	1.92(1) ×1
		⟨Mn3−O⟩	1.96	⟨Mn6−O⟩	1.91
		Δd	5.2×10^{-4}	Δd	6.8×10^{-4}

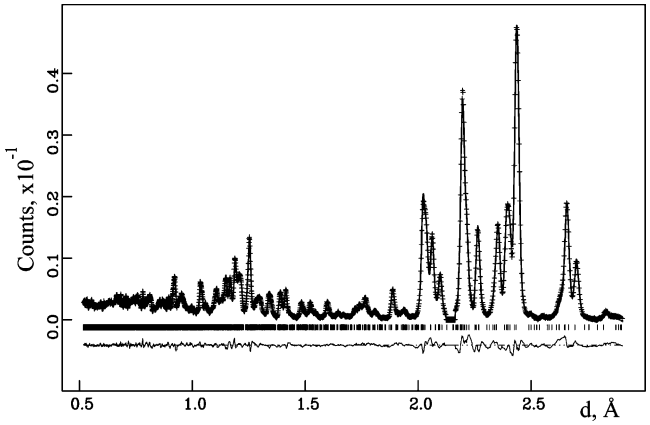

Figure 4. Experimental, calculated, and difference neutron powder difference profiles for $CaMn_3O_6$.

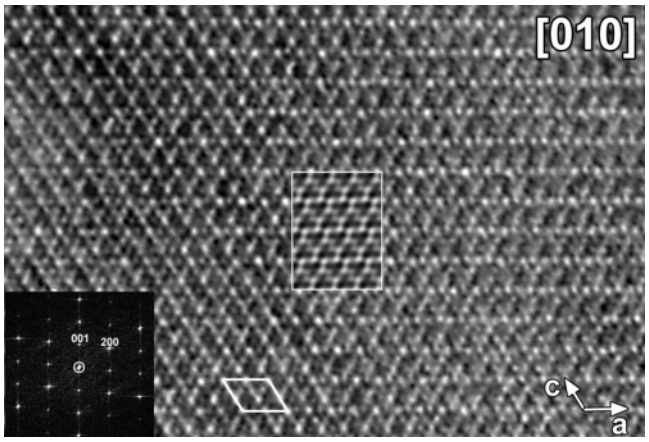

Figure 5. HREM image of $CaMn_3O_6$, taken along the [010] direction. The calculated image ($\Delta f = +300$ Å, $t = 40$ Å) is shown as an inset with a white border. The white paralellogram outlines one unit cell.

is found between the experimental and calculated images, supporting the determined crystal structure.

4. Structure Description

The $CaMn_3O_6$ crystal structure is based on a framework built of double chains of edge-sharing MnO_6 octahedra propagating along c_m. The chains are linked by common corners, producing six-sided tunnels, wherein the Ca^{2+} cations are located. Since the close resemblance between the $CaMn_3O_6$ framework and the $CaFe_2O_4$ prototype is obvious due to the identical geometry of the octahedral framework, the relationships between these two compounds are discussed first, and those with $CaMn_2O_4$ are then discussed further along with the different tunnel structures of the Ca−Mn−O system. The decrease of the symmetry down to monoclinic in $CaMn_3O_6$ is caused by the reduced number of A-cations in the tunnels, and the ordered distribution of vacant and occupied A-sites along the tunnels. In agreement with the amount of A-cations in $CaMn_3O_6$ with regard to the fully occupied tunnels of the ideal AM_2O_4 structure, every third A-position in the tunnels is vacant with a 1−2-type ordering of one vacancy and two cations. Empty A-sites in neighboring Ca chains at $x \approx 0.25$ and $x \approx 0.75$ are shifted with respect to each other along the c_m axis by one repeat period of the $CaFe_2O_4$ unit cell (Figure 6), which leads to the monoclinic superstructure. In the $CaMn_3O_6$ crystal structure

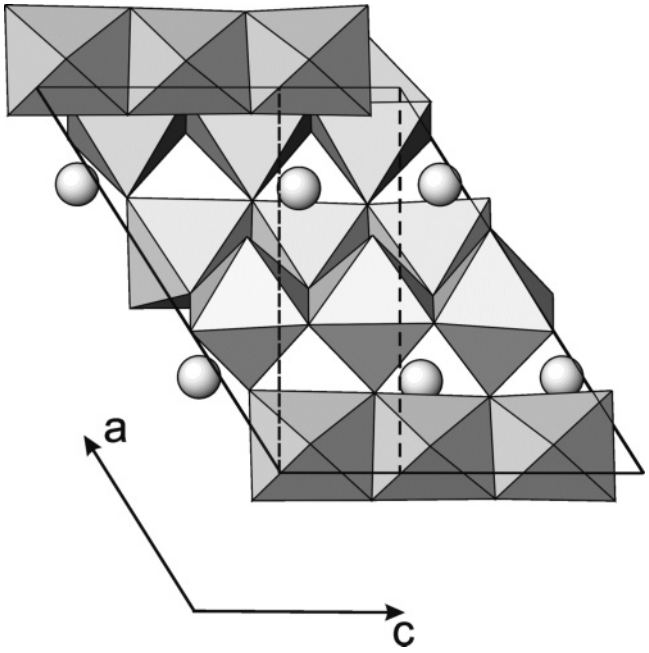

Figure 6. Slice of the $CaMn_3O_6$ structure near $y = 0.66$, viewed along the [010] direction. The $CaFe_2O_4$ subcell is marked with dashed lines.

the Ca atoms are situated in capped trigonal prisms (CN = 8) with Ca−O interatomic distances ranging from 2.23 to 2.64 Å.

The distortion of the octahedral environment and the average ⟨Mn−O⟩ interatomic distances for the Mn1, Mn2, Mn4, and Mn5 cations are slightly different from those for the Mn3 and Mn6 cations. This difference is reflected by the octahedral distortion parameter Δd, defined as[19]

$$\Delta d = (1/6) \sum_{n=1-6} [(d_n - d)/d]^2$$

where d_n are the individual Mn−O distances and d is the average ⟨Mn−O⟩ distance. The Mn3 and Mn6 cations are located in slightly distorted octahedral environments ($\Delta d = 5.2-6.8 \times 10^{-4}$) with ⟨Mn−O⟩ = 1.91−1.96 Å. The distortion of the $Mn1O_6$, $Mn2O_6$, $Mn4O_6$, and $Mn5O_6$ octahedra is stronger ($\Delta d = 0.4 \times 10^{-2}$ to 1.3×10^{-2}). The Mn1 and Mn2 cations show four shorter equatorial (1.85−2.08 Å) and two longer apical (2.21−2.39 Å) Mn−O bonds; the apical bonds are aligned perpendicular to the direction of the double-chain propagation. For the Mn4 and Mn5 cations only one apical bond is substantially longer (2.22−2.458 Å). The average ⟨Mn−O⟩ distance of 1.99−2.07 Å for the Mn1, Mn2, Mn4, and Mn5 cations is larger than that for the Mn3 and Mn6 cations (1.91−1.96 Å). One can speculate that the observed differences in the coordination environment are related to charge ordering; i.e., the dominantly trivalent Mn cations are situated preferentially at the Mn1, Mn2, Mn,4 and Mn5 positions, whereas the $Mn3O_6$ and $Mn6O_6$ octahedra have a dominantly tetravalent character. The Jahn-Teller distortion, intrinsic for the Mn^{3+} cations in a high spin state, and the larger ionic radius of Mn^{3+} ($r(Mn^{3+}) = 0.79$ Å, $r(Mn^{4+}) = 0.68$ Å[20]) account for

(19) Alonso, J. A.; Martinez-Lope, M. J.; Casais, M. T.; Fernandez-Diaz, M. T. *Inorg. Chem.* **2000**, *39*, 917.
(20) Shannon, R. D. *Acta Crystallogr.* **1976**, *A32*, 751.

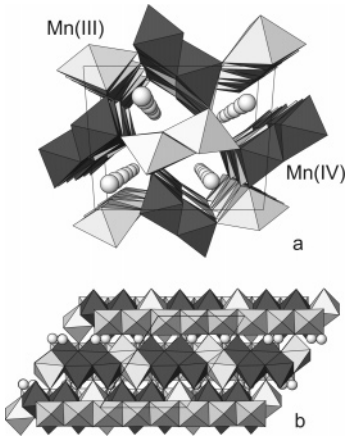

Figure 7. Tentative charge ordering scheme in $CaMn_3O_6$: (a) a chessboard pattern of double chains containing only trivalent Mn cations (light octahedra) and those containing both tetravalent and trivalent Mn cations (dark-shaded octahedra); (b) the location of the groups of four tetravalent Mn atoms along the double chains.

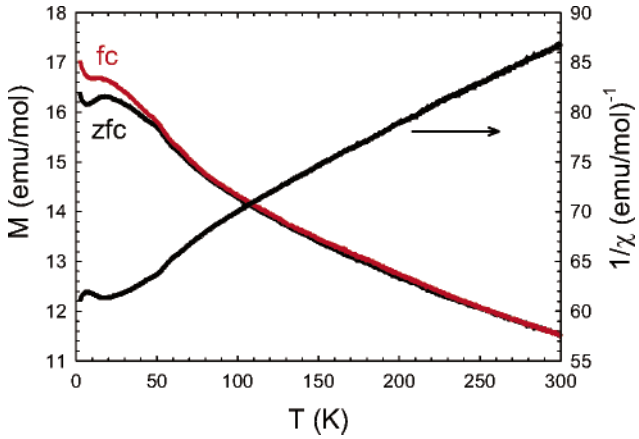

Figure 8. Magnetization curves (zfc and fc) recorded in a magnetic field of 0.1 T with the corresponding inverse (zfc) susceptibility curve.

the larger distortion and average ⟨Mn−O⟩ distance for the Mn1, Mn2, Mn4, and Mn5 cations. The average oxidation state of Mn in $CaMn_3O_6$, $V_{Mn} = +3.33$, is in agreement with the proposed distribution of the $Mn^{(3+\delta)+}$ and $Mn^{(4-\delta)+}$ cations over the crystallographic positions, which results in a formal $Mn^{3+}/Mn^{4+} = 2:1$ ratio. The double chains containing preferentially trivalent Mn cations and those with both tetravalent and trivalent Mn cations are arranged in a chessboard pattern being viewed along the *c*-axis (Figure 7a). Four $Mn^{(4-\delta)+}O_6$ octahedra are associated into groups, separated by two $Mn^{(3+\delta)+}O_6$ octahedra (Figure 7b); these groups are associated with the empty A-positions, thus having an impact on the charge compensation and stabilizing the structure.

5. Magnetic Properties

The magnetization curves (zfc and fc) recorded in a magnetic field of 0.1 T are given in Figure 8 with the corresponding inverse (zfc) magnetic susceptibility curve. The latter reveals the strong anti-ferromagnetic character of the sample, even if some ferro- or ferrimagnetic interactions could be responsible for the slight increase of the signal at low temperature and for the deviation between the zfc and fc magnetization curves. The high-temperature part of the inverse magnetic susceptibility curve can be linearly fitted with a Curie−Weiss law, leading to a $\mu_{eff} \approx 4.05\mu_B$ (per Mn atom), which is slightly lower than the expected value ($4.54\mu_B$) for $Mn^{3.33+}$ corresponding to the "ideal" formula $CaMn^{3+}{}_2Mn^{4+}O_6$. The inverse susceptibility curve deviates from linearity at a higher temperature (around 50 K) than the one observed by Glaunsinger et al.[15] Further investigation by low-temperature neutron diffraction is required to determine accurately the magnetic behavior of this compound. In fact, this point deserves attention due to the interesting structure of the compound in which ferromagnetic ($Mn^{3+}-O-Mn^{4+}$) and anti-ferromagnetic ($Mn^{3+}-O-Mn^{3+}$ and $Mn^{4+}-O-Mn^{4+}$) interactions will probably develop. As shown in Figure 7a, one kind of double chain consists of $Mn^{3+}O_6$ octahedra-sharing edges, whereas the two other double chains involve an alternation of $Mn^{3+}O_6-Mn^{4+}O_6-Mn^{4+}O_6$ octahedra sharing edges too. The links between these chains are made by $Mn^{3+}O_6-Mn^{4+}O_6$ and $Mn^{3+}O_6-Mn^{3+}O_6$ bridges that could lead to a frustrated state.

6. Structural Considerations and Concluding Remarks

Bearing in mind that $CaMn_2O_4$ is a distorted variant of $CaTi_2O_4$ with the same connectivity scheme of the metal−oxygen octahedra, the parameters governing the stabilization of the configuration of either a $CaTi_2O_4$ or $CaFe_2O_4$ framework with six-sided channels are not yet completely clear. Numerous oxides adopt the $CaFe_2O_4$-type form, whereas the only complex oxides adopting the $CaTi_2O_4$-type form are $CaTl_2O_4$ [21] and, indeed, the distorted $CaMn_2O_4$. The latter has been described as a chemical twin of a rock salt type structure. For example, let us consider two different mixed valent compact binary oxides, Eu_3O_4,[22] which adopts the $CaTi_2O_4$-type arrangement, and the high pressure form of Fe_3O_4 for which both $CaMn_2O_4$-type[23] and $CaTi_2O_4$-type[24] forms have been proposed. The formulations are therefore $Eu^{2+}{}_{0.5}Eu^{3+}O_2$ and $Fe^{2+}_{0.5}Fe^{3+}O_2$, thus highlighting that only trivalent cations are present in the octahedral framework. The comparison of $CaTl_2O_4$ ($CaTi_2O_4$ type) with its analogue $SrTl_2O_4$ ($CaFe_2O_4$ type) demonstrates that the presence of larger cations in the tunnels can enforce the structure to adopt the $CaFe_2O_4$-type arrangement.[25] However, it is obvious that a mismatch between the B−O and A−O bonds in the $A_xB_2O_4$ tunnel oxides cannot be the only factor determining the relative stability of these two structure types. The fact that the $CaMn_2O_4$ and $CaFe_2O_4$ structures are obtained for cations of very similar size ($r(Mn^{3+}) = 0.65$ Å, $r(Fe^{3+}) = 0.645$ Å[20]) makes it clear that electronic factors should play an important role. It was shown that the high pressure form of $CaMn_2O_4$ is a *Bbmm* $CaTi_2O_4$ form;[26] the effect of pressure reduces the structure distortion, leading to a decrease of the volume and a reduction of the Jahn-Teller effect of the Mn^{3+} cations.

(21) Goutenoire, F.; Caignaert, V.; Hervieu, M.; Michel, C.; Raveau, B. *J. Solid State Chem.* **1995**, *114*, 428.
(22) Barnighausen, H.; Brauer, G. *Acta Crystallogr.* **1962**, *15*, 1059.
(23) Fei, Y.; Frost, D. J.; Mao, H. K.; Prewitt, C. T.; Hauserman, D. *Am. Mineral.* **1999**, *84*, 203.
(24) Haavik, C.; Stolen, S.; Fjellvag, H.; Hanfland, M.; Hausermann, D.; *Am. Mineral.* **2000**, *85*, 514.
(25) Michel, C.; Hervieu, M.; Caignaert, V.; Raveau, B. *Acta Crystallogr.* **1992**, *C48*, 1747.
(26) Wang, Z.; Saxena, S. K.; Neumeier, J. J. *J. Solid State Chem.* **2003**, *170*, 382.

An interesting point is the stabilization of two structural forms within the Ca−Mn−O system, i.e., $CaMn_2O_4$ with a $CaTi_2O_4$-type structure and $CaMn_3O_6$ with a $CaFe_2O_4$-type structure. For easier comparison, use of the $A_xMn_2O_4$ notation allows us to consider the amount of inserted cations A_x ($A = Ca^{2+}$) in the octahedral framework. In this case, $CaMn_3O_6$ corresponds to $Ca_{2/3}Mn_2O_4$. Two factors may be responsible for the significant decrease of the unit cell volume on going from $CaMn_2O_4$ (305.57 Å^3 [12]) to $Ca_{2/3}Mn_2O_4$ (289.475 Å^3 (present work)): the decreasing Ca content and the increasing manganese valence, from Mn^{3+} to $Mn^{3.33+}$, in agreement with the cation radii.[20] Besides the pure cation size effect, the introduction of Mn^{4+} in the octahedral framework reduces the deformation of the MnO_6 octahedra.

The "charge ordering" effect resulting from the coexistence of Mn^{3+} and Mn^{4+} is another interesting point, which of course does not exist in $CaMn_2O_4$. It should be noted that bond valence sum calculations lead to values, which do not correspond to the exact values of +3 and +4 for the manganese cations. Indeed, charge localization in a charge ordered state in manganites is never complete and usually the degree of disproportionation does not exceed 0.1−0.2 e^- so that the actual valence state of the Mn cations is better expressed as $Mn^{(3.33\pm\delta)+}$.

In conclusion, the discovery of both cation/vacancy and charge ordering in $CaMn_3O_6$ leads us to investigate the actual origin of these phenomena, specifically exploring its high-temperature behavior and optimization of the synthesis process. This work is now in progress.

Acknowledgment. The work was supported in part by the IAP V-1 program of the Belgium government and the RFBR projects 04-03-32785-a and 05-03-34812-MF-a. L.J.G. gratefully acknowledges the European Union for a fellowship (SCOOTMO: HRPN-CT-2002-00293.). We are grateful to Winfried Kockelman for the neutron powder diffraction measurements.

Supporting Information Available: An X-ray crystallographic file (CIF). This material is available free of charge via the Internet at http://pubs.acs.org.

CM0618998